Secondary ELM filaments in the National Spherical Torus Experiment

R. J. Maqueda [a], R. Maingi [b], J.-W. Ahn [c], NSTX Team

[a] Nova Photonics Inc., Princeton, NJ 08540, USA

[b] Oak Ridge National Laboratory, Oak Ridge, TN 37831, USA

[c] University of California at San Diego, La Jolla, CA 92093, USA

Filamentary structures are observed in the scrape-off layer of the National Spherical Torus Experiment during ELMs. While the early filaments correspond to a direct result of the ELM event, the “secondary” filaments which occur generally later but still within 1 ms of the ELM onset are observed to have the same characteristics as inter-ELM filaments (or blobs): poloidal auto-correlation lengths of ~4 cm and broadband frequency and poloidal wave number spectra. At the same time, no modes are observed during the phase in which secondary filaments are present.

1. Introduction

The large pressure gradients near the edge of tokamak experiments during H-mode operation are prone to periodic instabilities known as Edge Localized Modes (ELM). A fraction of the energy and particles lost across the separatrix and near scrape-off layer (SOL) is associated with filamentary structures that are aligned with the local magnetic field and propagate radially outwards [1]. The perturbed edge profiles due to the ELM, including a momentary loss of the E_r well present during H-mode confinement [2], can result in enhanced transport and be also responsible for energy and particle losses. It has been observed in Alcator C-Mod that during the ELM event there are primary and secondary filaments that propagate radially in the SOL [3], with the primary filaments perhaps being more closely related to the instability driving the ELM and the secondary filaments possibly related to the enhanced transport. Recently, the study of the filament characteristics has found that the initial low-n structure is followed by a "quasi-mode" structure with an increased toroidal mode number [4].

This paper presents experimental results from the National Spherical Torus Experiment (NSTX) on filaments present in the SOL during Type I and Type III ELMs [5], with emphasis on secondary filaments. The experimental setup and main characteristics of the plasmas in NSTX are presented in Section 2. The characteristics of the secondary filaments is presented in Section 3 and the paper concludes with a brief discussion in Section 4.

2. Experimental setup

The experiments were carried out in the National Spherical Torus Experiment (NSTX) [6]. This experiment is a low aspect ratio tokamak with a major radius $R = 0.86$ m and a minor radius $a = 0.67$ m where, for the discharges discussed in this paper, a plasma current of $I_p = 800$ kA, a toroidal field on axis of $B_t = 0.45$ T and an elongation of $\kappa \sim 1.9$ were used in a magnetic topology close to double null ($\Delta r_{sep} \sim 3$ mm biased towards the lower divertor). Regimes with periodic Type I and Type III ELMs were achieved by adjusting the auxiliary heating power by means of neutral beam injection to 4.7 MW and 2 MW, respectively. This resulted in ELM frequencies of

~120 Hz for Type I ELMs and ~460 Hz for Type III ELMs. In both cases the energy lost per ELM is below the 2% measurable with the equilibrium fit reconstruction employed. The ELM classification into different types is based on their size and frequency scaling.

The main diagnostic used in this work was high frame rate imaging in the visible range of wavelengths. Two fast-framing digital cameras were employed, each capturing 121212 frames/s [7]. One of the cameras, a Phantom 7.3 from Vision Research, was used in a wide-angle, fish-eye elevation view of the plasma covering about 90% of the plasma cross-section, centered up and down respect to the device midplane. The other camera (a Phantom 7.1) viewed a tangential, zoomed-in view of a ~24 cm poloidal section of the edge just above the outer midplane of the plasma. The pitch angle of the magnetic field in the viewing region of this tangential edge camera was selected so that the visible light emission was viewed along the direction of the local magnetic field line and in this way obtain "end-on" imaging of the field-aligned filamentary structures. In addition, a deuterium gas puff was added in the field of view of the edge camera to further localize the emitting region to a ~20 cm depth and also increase the contrast and brightness of the D_α line emission which was selected with a narrowband interference filter. Further details of this gas puff imaging (GPI) diagnostic can be seen in Ref. [8]. Although no interference filter was used in the wide-angle viewing camera, most of the emission recorded corresponds to deuterium line emission from the edge and SOL. Finally, even though the cameras were run independently with no frame synchronization, the overlapping fields of view were employed to maintain a cross-reference between the two independent time bases and correct for any slow time drifts.

3. Secondary ELM filaments

While there is considerable variability in the overall filament structure observed between ELMs of the same type some general features can be distinguished. An example of a Type III ELM is shown in Fig. 1. In this case 4 primary filaments, indicated by green arrows in frame #6 of Fig. 1(a), grow independently in ~30 μs. This structure is similar to results previously reported by numerous authors [1,5]. The filament on the right edge of this frame can be seen "end on" in the corresponding edge view image [frame #6 of Fig. 1(b)] having evolved from the unperturbed H-mode edge. A precursor

filament structure, rotating in the direction of the core rotation (co-I_p) at ~1 kHz can sometimes be seen. In a similar way to other experiments [1], the primary filaments propagate radially outwards and poloidally in the ion diamagnetic drift direction (downwards in this case) as seen in Fig. 1(b), frames #5-#9. Generally, due to the break-up of the primary filaments, the edge continues to develop into further filaments and hence an increased toroidal "mode number" (similar the results of Ref. [4]), resulting in a fine structured filament pattern (frame #9). The edge, perturbed by the ELM, is then subject to increased turbulence and blob generation as seen in the subsequent frames of Fig. 2(b) resulting in an even higher toroidal "mode number" since these turbulent blobs are also aligned with the local magnetic field. These later structures are the secondary filaments corresponding to this Type III ELM event. Secondary filament activity decays in ~200 μs after the first onset of the ELM, recovering the typical H-mode edge seen in frames #1-#2.

The characteristics of the D_α emission in the SOL, which is due to a non-linear relationship with the local n_e and T_e [9], can be seen in Figs. 2 and 3. The early post-ELM emission for Type III ELMs is relatively larger than for Type I ELMs, as seen in Fig. 2(a), due to the primary filaments typically reaching far into the SOL while in Type III ELMs they break out within 3 cm of the separatrix. The Type III ELM emission then decays faster (τ ~ 150 μs) than for Type I's which maintain a high level in the SOL for about 300 μs followed by a slower decay (τ ~ 300 μs). In both ELM types the emission is not uniform along the poloidal dimension but composed of secondary small scale filaments as seen in Fig. 1(b), frame #19 and higher. The poloidal auto-correlation length (FWHM) being ~4 cm for both types of ELMs as seen in Fig. 2(b), and not different than the lengths for inter-ELM and L-mode turbulence born filaments (see for instance, Fig. 6 of Ref. [10]).

In Fig. 3 the spectral analysis in both time and poloidal scale domain is shown for Type I ELMs and compared with the corresponding inter-ELM spectra. In both plots the difference between the secondary ELM filaments and the inter-ELM filaments (turbulence born) can be best characterized as a uniform increase in the spectral amplitude without the appearance of modes, neither in time nor space. In both spectra

there is a broad distribution of power among frequencies and the poloidal wave numbers (k_{pol}).

The velocities of the post-ELM filaments are shown in Fig. 4. While primary filaments, occurring in the first 40 μs after ELM onset, can reach velocities of 7 km/s and higher in either component (v_r or v_{pol}), secondary ELM filaments have typical velocities of 1-2 km/s. These velocities are also characteristics of turbulence born filaments (i.e., blobs) [10]. It should also be noted here that fast moving primary filaments are more prevalent at this radial location in Type III ELMs than on Type I ELMs.

4. Discussion

In the preceding Section it is shown that the primary ELM filaments present in the SOL are followed by a period of fine structured secondary filaments. These later filaments have all of the characteristics of turbulence born filaments (or blobs) [*] and, in contrast, do not present characteristics of periodic modes. A similar conclusion was reached in the TCV tokamak, although primary filaments were not seen in that experiment [11]. The edge instability giving rise to the ELM event, or as a consequence of this event, modifies the edge profiles in a manner that increases the turbulence that gives rise to the intermittent blobs. At the same time it has been shown in other experiments that the primary filaments themselves carry only a small fraction of the ELM energy loss [1]. The remaining loss is due to transport enhanced by modified edge profiles or due to draining of core plasma during a short period of time $\tau_{ELM} \approx \left(\tau_A^2 \tau_E\right)^{1/3}$ along the primary filaments as proposed in Ref. [1]. While, as presented here, a component of the post-ELM enhanced transport may be due to intermittent events it has been shown that blob phenomena have, in ELM free periods or L-mode, a non-negligible contribution on the cross-field transport process [12]. In summary then, the contribution that intermittent (secondary filaments) vs. diffusive transport has in this phase of the ELM event need to be evaluated since they have different consequences on the energy and particle deposition profiles over plasma facing components.

Some of the characteristics of the secondary ELMs presented in this paper are also observed with edge Langmuir probes in NSTX as well as other experimental devices [4,13-14]. Caution should then be exercised when interpreting the intermittent events

observed with probes as some of them (the later ones) may be due to “turbulent blobs” and may not be directly associated to the instability causing the ELM. A similar caution should be exercised when imaging the ELM phenomena with cameras or other diagnostics that don’t posses enough time resolution to differentiate between primary and secondary filaments.

Acknowledgments

This work was supported by US D.O.E. Contract Nos. DE-FG02-04ER54520, DE-AC05-00OR22725 and DE-AC02-76CH03073.

References

[1] A. Kirk, *et al.*, Plasma Phys. Control. Fus. 49 (2007) 1259.

[2] M. R. Wade, *et al.*, Phys. Rev. Lett. 94 (2005) 225001.

[3] J. L. Terry, *et al.*, J. Nucl. Mater. 363-365 (2007) 994.

[4] J. Neuhauser, *et al.*, Nucl. Fusion 48 (2008) 045005.

[5] R. Maingi, *et al.*, Nucl. Fusion 45 (2005) 1066.

[6] J. E. Menard, *et al.*, Nucl. Fusion 47 (2007) S645.

[7] R. J. Maqueda, *et al.*, J. Nucl. Mater. 363-365 (2007) 1000.

[8] R. J. Maqueda, *et al.*, Rev. Sci. Instrum. 74 (2003) 2020.

[9] D. P. Stotler, *et al.*, J. Nucl. Mater. 314-316 (2003) 1066.

[10] S. J. Zweben, *et al.*, Nucl. Fusion 44 (2004) 134.

[11] R. A. Pitts, *et al.*, Proc. 34th EPS Conf. on Plasma Phys., ECA 31F (2007), P-2.026.

[12] J. A. Boedo, *et al.*, Phys. Plasmas 10 (2003) 1670.

[13] J. A. Boedo, *et al.*, J. Nucl. Mater. 337-339 (2005) 771.

[14] R. A. Pitts, *et al.*, Nucl. Fusion 47 (2007) 1437.

Figure Captions

Fig. 1. Filament structure in Type III ELM (shot 124667): (a) Wide angle view from 262.542 ms (frame #1) to 262.633 ms (#12) and (b) edge view from 262.543 ms (frame #1) to 262.905 ms (#45). The first 12 frames in (a) and (b) were obtained at the same time. For contrast enhancement, an average image before the ELM is subtracted from the wide view images. Each of the images in (b) corresponds to a 24 cm x 24 cm portion of the radial vs. poloidal plane in the high field side of the torus just above the midplane (cyan box in frame 1, part (a)). The solid line in (b) indicates the separatrix and the dotted lines the limiter shadow.

Fig. 2. Post-ELM evolution of (a) D_α emission and (b) Poloidal auto-correlation length in the SOL ($R-R_{sep} \sim 5.5$ cm). Traces correspond to ensemble averages of 17 Type I ELMs or 19 Type III ELMs and the dotted lines represent the standard deviation of these ensembles. Part (a) is normalized by the inter-ELM emission at that particular radius.

Fig. 3. Spectra of D_α emission in the SOL ($R-R_{sep} \sim 5.5$ cm) in the (a) time domain and (b) poloidal spatial domain for the same database of 17 Type I ELMs used in Fig. 2. The time interval $0.1 \text{ ms} < t - t_{ELM} < 0.3 \text{ ms}$ where the ensemble average emission is approximately constant (Fig. 2(a)) in time is used.

Fig. 4. Velocity of filaments as they cross the $R-R_{sep} \sim 2.5$ cm surface of the GPI viewing plane (edge view): (a) radial velocity component and (b) poloidal velocity component. A negative poloidal velocity indicates a downward movement, in the direction of the ion diamagnetic drift.

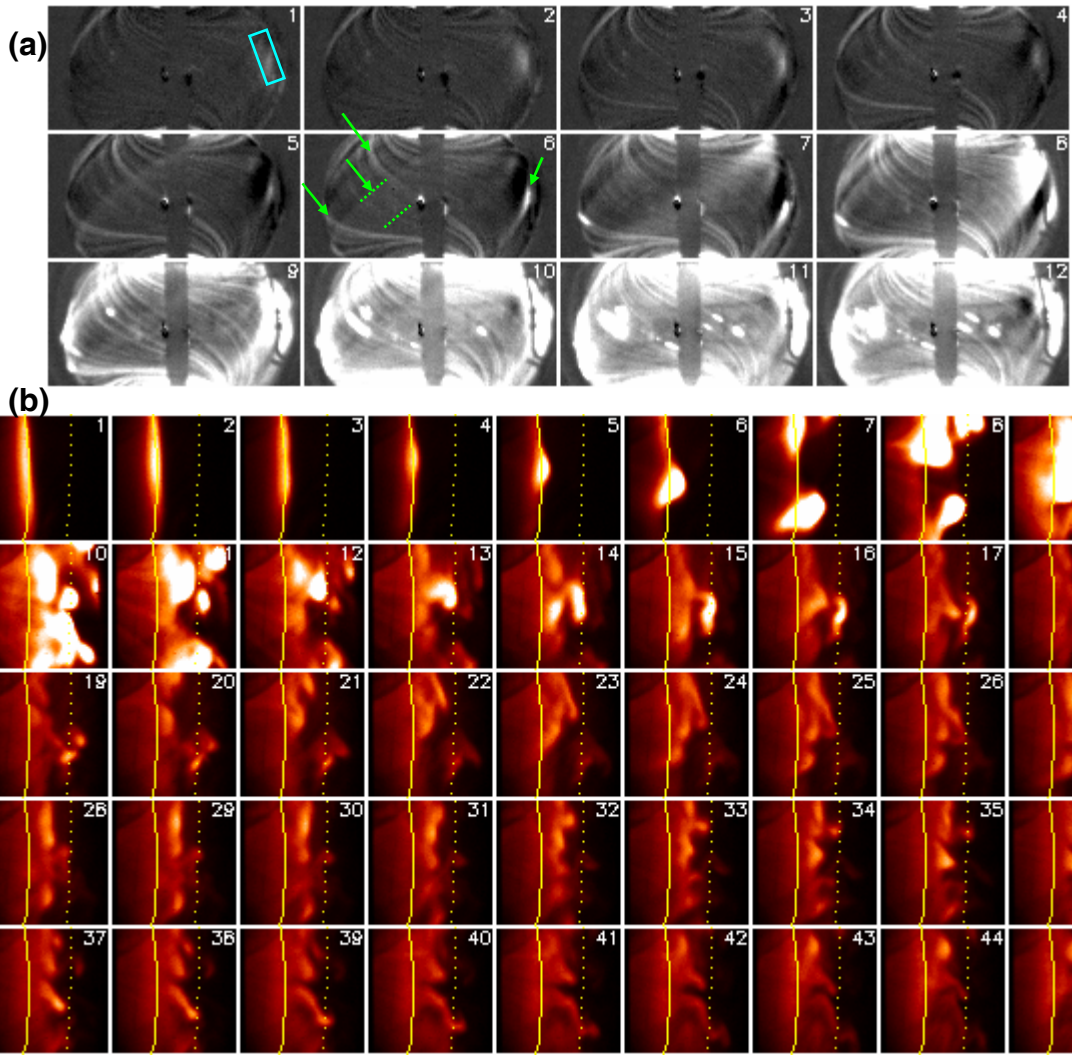

Fig. 1

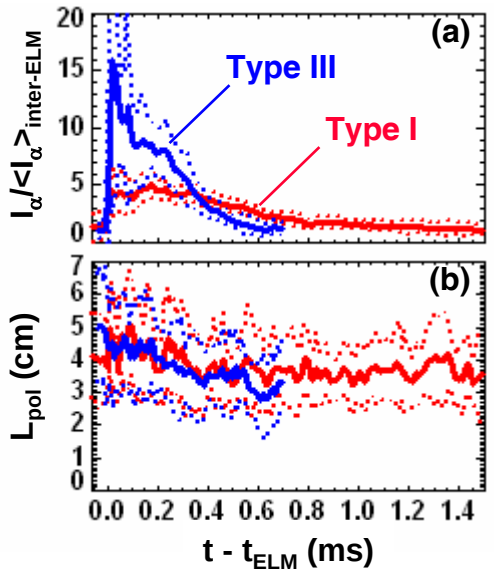
(a)
Type III
Type I
$I_\alpha/\langle I_\alpha \rangle_{inter\text{-}ELM}$
(b)
L_{pol} (cm)
$t - t_{ELM}$ (ms)

Fig. 2

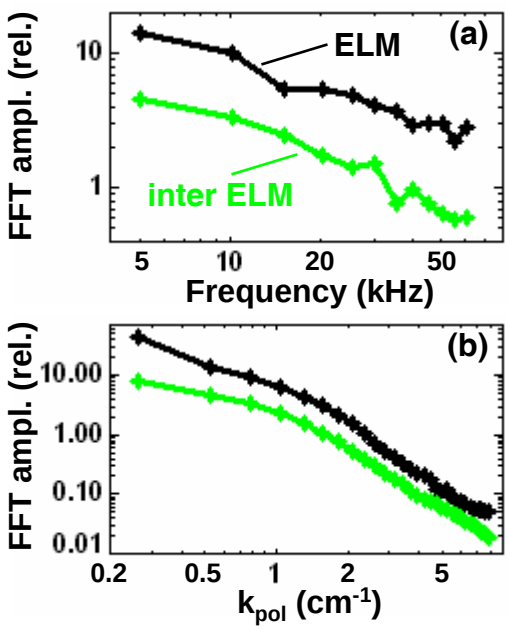
FFT ampl. (rel.)
10
1
ELM
(a)
inter ELM
5
10
20
50
Frequency (kHz)
FFT ampl. (rel.)
(b)
10.00
1.00
0.10
0.01
0.2
0.5
1
2
5
k_pol (cm^-1)

Fig. 3

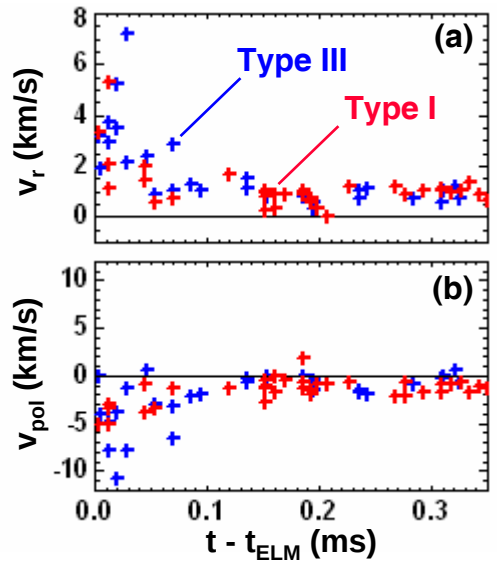
(a)
Type III
Type I
v_r (km/s)
8
6
4
2
0
(b)
v_{pol} (km/s)
10
5
0
-5
-10
0.0
0.1
0.2
0.3
t - t_{ELM} (ms)

Fig. 4